



Full Text View

[Volume 32, Issue 12 \(December 2002\)](#)

Journal of Physical Oceanography

Article: pp. 3657–3670 | [Abstract](#) | [PDF \(1.30M\)](#)

Buoyancy and Mixed Layer Effects on the Sea Surface Height Response in an Isopycnal Model of the North Pacific

LuAnne Thompson

School of Oceanography, University of Washington, Seattle, Washington

Kathryn A. Kelly

Applied Physics Laboratory, University of Washington, Seattle, Washington

David Darr

School of Oceanography, University of Washington, Seattle, Washington

Robert Hallberg

NOAA/Geophysical Fluid Dynamics Laboratory, Princeton, New Jersey

(Manuscript received August 16, 1999, in final form July 25, 2002)

DOI: 10.1175/1520-0485(2002)032<3657:BAMLEO>2.0.CO;2

ABSTRACT

An isopycnal model of the North Pacific is used to demonstrate that the seasonal cycle of heating and cooling and the resulting mixed layer depth entrainment and detrainment cycle play a role in the propagation of wind-driven Rossby waves. The model is forced by realistic winds and seasonal heat flux to examine the interaction of nearly annual wind-driven Rossby waves with the seasonal mixed layer cycle. Comparison among four model runs, one adiabatic (without diapycnal mixing or explicit mixed layer dynamics), one diabatic (with diapycnal mixing and explicit mixed layer dynamics), one with the seasonal cycle of heating only, and one with only variable winds suggests that mixed layer entrainment changes the structure of the response substantially, particularly at midlatitudes. Specifically, the mixed layer seasonal cycle works against Ekman pumping in the forcing of first-mode Rossby waves between 17° and 28°N. South of there the mixed layer seasonal cycle has little influence on the Rossby waves, while in the north, seasonal Rossby waves do not propagate. To examine the first baroclinic mode response in detail, a modal decomposition of the numerical model output is done. In

Table of Contents:

- [Introduction](#)
- [The isopycnal model formulation](#)
- [The role of diapycnal](#)
- [Modal decomposition and](#)
- [Conclusions](#)
- [REFERENCES](#)
- [APPENDIX](#)
- [TABLES](#)
- [FIGURES](#)

Options:

- [Create Reference](#)
- [Email this Article](#)
- [Add to MyArchive](#)
- [Search AMS Glossary](#)

Search CrossRef for:

addition, a comparison of the forcing by diapycnal pumping and Ekman pumping is done by a projection of Ekman pumping and diapycnal velocities on to the quasigeostrophic potential vorticity equation for each vertical mode. The first baroclinic mode's forcing is split between Ekman pumping and diapycnal velocity at midlatitudes, providing an explanation for the changes in the response when a seasonal mixed layer response is included. This is confirmed by doing a comparison of the modal decomposition in the four runs described above, and by calculation of the first baroclinic mode Rossby wave response using the one-dimensional Rossby wave equation.

- [Articles Citing This Article](#)
- Search Google Scholar for:
- [LuAnne Thompson](#)
 - [Kathryn A. Kelly](#)
 - [David Darr](#)
 - [Robert Hallberg](#)

1. Introduction

The TOPEX/Poseidon altimeter observations of SSH (sea surface height) show a variety of responses to atmospheric forcing and give information about how the ocean adjusts to this forcing. The SSH observations can be explained primarily by the adjustment of the ocean to seasonal variations of wind and heat-flux forcing ([Chelton and Schlax 1996](#); [Vivier et al. 1999](#), VKT hereafter; [Stammer 1997](#); [Stammer et al. 1996](#), Plate 3). Studies in the North Pacific show that the steric response to heating is large at high latitudes ([VKT](#); [Stammer 1997](#)). A quasi-steady topographic Sverdrup balance is also found over the North Pacific to latitudes as low as 25°N. Equatorward of that, the flat-bottomed Sverdrup balance is important ([VKT](#)). Forced first-mode baroclinic Rossby waves are seen to propagate south of about 40°N.

A feature of the observed Rossby waves not explained by the simple models is apparent damping of Rossby waves as they propagate from east to west across the basin. [Qiu et al. \(1997\)](#) show that Laplacian or biharmonic mixing should be added to the simple long-wave model for better agreement with SSH observations. This form of damping represents lateral mixing by eddies, and is scale selective. Another possible form of damping is Newtonian cooling proportional to SSH in a reduced gravity model. This formulation could represent simple thermal damping of the SSH, assuming SSH is proportional to SST. Newtonian damping is also interpretable as potential vorticity mixing, indicative of vertical mixing processes in the ocean. This suggests that diabatic effects may play a role in the dynamics of the response of the ocean to variability in wind forcing.

In reduced gravity models of the ocean's response to wind forcing ([Qiu et al. 1997](#)), many physical processes are ignored; these include the coupling of the Rossby waves to bottom topography ([Killworth and Blundell 1999](#)), coupling among different vertical modes, and vertical mixing processes. More sophisticated numerical models include these effects but are difficult to interpret. Here we focus on the influence of diapycnal processes, primarily the seasonal cycle of entrainment and detrainment of the mixed layer, on the large-scale response of the ocean to both wind and heat-flux forcing by doing a series of model runs with different forcing configurations. The possibility of forcing of Rossby waves by diapycnal processes has been explored previously in the context of decadal variability ([Liu 1999](#)). With simplified geometry and forcing, Liu finds that Ekman pumping forces the first baroclinic mode, while heating and cooling at the surface primarily forces the second baroclinic mode. Here we quantify these results in a model that has realistic forcing to determine if vigorous mixing associated with the seasonal evolution of the mixed layer influences the first baroclinic mode evolution and thus the SSH in the ocean.


The outline of the paper is as follows. The numerical model used in this study is described in [section 2](#). Four model runs are discussed in [section 3](#). The dynamics at work are explored in the context of a quasigeostrophic modal decomposition of the oceanic response in [section 4](#). Consequences of the results for the interpretation of the response of the ocean to seasonal forcing are discussed in [section 5](#).

2. The isopycnal model formulation

The model used for this study is the Hallberg Isopycnal Model ([Hallberg 2000](#); [Hallberg and Rhines 1996](#); [Ladd and Thompson 2001](#)), an isopycnal model similar to MICOM [[New et al. \(1995\)](#) and references therein]. The model includes diapycnal mixing and an embedded mixed layer. The mixed layer has Kraus–Turner physics with additional shear-dependent mixing below the mixed layer, and the entrainment algorithm used in MICOM. However, detrainment occurs through a buffer layer, an additional layer with variable density. The detrainment method is described in detail in the [appendix](#) and has been used to study the seasonal cycle and water mass formation ([Ladd and Thompson 2001](#)).


To maintain the model's free surface while increasing the time step, the value of gravity at the free surface is 10 times smaller than the actual value. The SSH response is 10 times larger than what it would be in the ocean so that in all plots of SSH from the model, we divide the magnitudes by 10. High-frequency barotropic motions will not be well represented in the model, owing to both the artificial value of g as well as the closed domain. An experiment with the true value of g was done

and compared against the control run described below for year 1992. The response is quantitatively similar, with rms SSH locally no more than 10% larger. The low-frequency (annual period) motions of interest are very well represented by the approximation used here. In particular, quasi-steady barotropic topographic Sverdrup response on the annual period is well reproduced in the model, as demonstrated by [VKT](#).



The model domain is the North Pacific between 13°S and 60°N. Resolution is 2° in each direction. The horizontal mixing is biharmonic (with the coefficient set at $2 \times 10^{15} \text{ m}^4 \text{ s}^{-1}$), which favors mixing at smaller lateral scales. Thus, the solution is less viscously controlled than one with the numerically required value of Laplacian mixing. The diapycnal mixing coefficient is $1 \times 10^{-5} \text{ m}^2 \text{ s}^{-1}$ unless otherwise noted. There is also horizontal thickness diffusion of $20 \text{ m}^2 \text{ s}^{-1}$, required for numerical stability. Bathymetry is taken from ETOPO 60. The model is forced by National Centers for Environmental Prediction (NCEP) daily wind fields, using perpetual 1992 winds to spin up the model for 20 years from the September initial conditions based on [Levitus et al. \(1994\)](#) and [Levitus and Boyer \(1994\)](#). Year 1992 is used for sensitivity studies. The buoyancy forcing is a combination of [da Silva et al. \(1994\)](#) heat fluxes and a relaxation to Levitus et al. sea surface buoyancy. The timescale of the relaxation is 100 days for a mixed layer 100 m thick ([Rothstein et al. 1998](#)). The coefficient of thermal expansion varies with location and season so that the equation of state is nonlinear in temperature. Two different density layer configurations are used ([Table 1](#) ). In the first case, an adiabatic simulation is done with 7 isopycnal layers. In the second, 8 isopycnal layers are used along with a buffer layer and a mixed layer, giving a total of 10 layers.

3. The role of diapycnal and mixed layer processes

To elucidate the role of diapycnal processes in the response of the ocean to seasonal forcing, we present the results from four model runs, run 1: wind forcing but no diapycnal processes either in the mixed layer or the interior and no heat flux forcing; run 2: heat flux, wind forcing, and interior diapycnal mixing; run 3: wind forcing but heat flux is given by relaxation to the annually averaged SST and wind mixing is turned off in the mixed layer; and run 4: seasonal heat flux forcing and annual mean wind stress. For run 3 and run 4, the models were run for several years from the spunup version of run 2. This ensures that the mean density structure is similar to that in run 2. In general, the model runs do not reproduce the smallest zonal scales seen in the observations ([Chelton and Schlax 1996](#); [Stammer 1997](#); [Stammer et al. 1996](#)). This occurs for two reasons: one is that the model is low resolution and the other is that there may not be sufficient energy at small scales in the wind fields.

We first examine the Rossby waves in runs 1 and 2. By Rossby waves, we mean the first baroclinic mode Rossby waves, identifiable by their westward phase propagation and distinct phase speed. A comparison shows that Rossby waves propagate more freely in run 1 at all latitudes and the response is larger ([Fig. 1](#) ). For both model runs, the rms SSH is lower than in the observations at low latitudes and comparable to the observations at midlatitudes. [VKT](#) showed that poleward of 25°N, the barotropic topographic Sverdrup balance is important and this part of the response appears to be well simulated in the model. In run 2 Rossby wave generation and propagation is inhibited relative to that in run 1 at midlatitudes. In fact, the rms model response in run 1 is as large or larger than in the observations at midlatitudes, despite the lack of a seasonal steric response. This result echoes that found by [Qiu et al. \(1997\)](#) in a one-dimensional wave equation where mixing was needed to better reproduce the observations.

The rms SSH is about a factor of 2 smaller than the observations in run 2 when the comparison is made after applying a correction for non-Boussinesq effects suggested by [Greatbatch \(1994\)](#) (see also [Stammer 1997](#)), proportional to the area-averaged heating. In the higher-resolution simulations of [Stammer et al. \(1996\)](#), the rms response is also a factor of 2 too small when compared with the observations. This result suggests that higher horizontal or vertical resolution is needed or the winds that forced the model had too low amplitude. In addition, the relaxation part of the heat flux could cause damping of the wind-driven signal, although we find that this is not the case here.

Of course, the response at the sea surface is not the only feature of the model ocean that changes when diabatic processes are included. There are profound differences in the density structure ([Fig. 2](#) ). In run 1, the density does not show a significant seasonal cycle. In addition, there are regions where the isopycnals are packed together (see for instance [Fig. 2c](#)  at 140°E). Water can be moved to different parts of the basin within the same layer but cannot cross layer interfaces. Convergences and divergences control the density structure and create regions with large vertical density gradients. In run 2, however, the density structure must be compatible with the surface buoyancy forcing. Density sections from the Levitus et al. climatology show layer thicknesses that are more uniform with longitude, with isopycnals depressed in the west, showing reasonable agreement with run 2. The mixed layer tends to be too deep in the model, most likely owing to incompatible heat fluxes and a lack of density resolution in the thermocline, especially at low latitudes and the Kraus–Turner mixed layer model formulation ([Ladd and Thompson 2001](#)).

Run 2 results are very robust to change of interior mixing values. When the interior diapycnal mixing is 10 times larger, and 10 times smaller, the SSH is very similar. It appears that it is the mixed layer evolution that plays a large role in how the Rossby waves propagate and evolve in the model rather than interior diapycnal mixing. Two additional runs were done to show that the relaxation part of the buoyancy flux as well as thickness diffusion have very little impact on the evolution of

the SSH.

In run 3 with heating only, we find that the rms SSH is relatively small, ensuring that the differences that we see between runs 1 and 2 are not simply because of a seasonal steric response (Fig. 3). There is however a striking difference between run 2 and run 4 from 18°N to 38°N where the run 4 response is almost twice as large as the run 2 response. Elsewhere, the two simulations are very similar, and both give smaller responses when compared to run 1.

4. Modal decomposition and the forcing of Rossby waves by diapycnal processes

So the question becomes, what is it about midlatitudes when the seasonal cycle in heating and cooling is included that causes the changes in the oceanic response? We know from previous work that north of about 40°N, the barotropic and steric response dominate on seasonal time scales (VKT) and neither of these responses should be influenced by diapycnal pumping that results from the entrainment/detrainment cycle of the mixed layer. However, the baroclinic modes could be influenced by diapycnal pumping (Liu 1999). To answer the above question, a modal decomposition is done to determine the relative contributions to the SSH from each vertical mode and then to examine the response of the first baroclinic mode under different forcing conditions. This allows the separation of the seasonal heating and barotropic response from the Rossby waves.

To do the modal decomposition, the annual mean stratification (layer thicknesses) and densities are used at each point. Care must be taken in constructing the annual mean stratification when layers vanish. Using the model results, a mean distribution of layer thicknesses is constructed such that each layer is of finite thickness, removing layers when they are less than 10 m from the mean field by combining layers. This results in some regions of the model ocean where fewer than 10 layers are used for the modal calculations. Interface deviations are constructed to be consistent with this algorithm. We do the modal decomposition locally, assuming that the motions are linear, and thus make the WKB approximation. A dynamically consistent way to decompose the response in the model is to use the vertical structure equation [see section 2 of Killworth et al. (1997) for the continuously stratified version of this]. In the layered framework, the vertical structure equation and the boundary conditions reduce to

$$\frac{\phi_1 - \phi_2}{H_1 g_1} + \frac{\phi_1}{H_1 g} + \frac{1}{c^2} \phi_1 = 0 \quad (1)$$

for the top layer,

$$\frac{(\phi_n - \phi_{n+1})}{H_n g_n} + \frac{(\phi_n - \phi_{n-1})}{H_n g_{n-1}} + \frac{1}{c^2} \phi_n = 0 \quad (2)$$

for the n th interior layer, and

$$\frac{(\phi_m - \phi_{m-1})}{H_m g_{m-1}} + \frac{1}{c^2} \phi_m = 0 \quad (3)$$

for the bottom layer, where m is the number of layers. In this framework, the streamfunction is related to interface displacements by

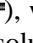
$$f \phi_n = g \hat{h}_0 + \sum_{i=1}^{n-1} f_i \hat{h}_i. \quad (4)$$

Here H_n is the mean thickness of layer n , ϕ_n is the streamfunction deviation from the mean streamfunction in layer n , and g_n is the reduced gravity between layer n and layer $n - 1$ taken from the mean density profile. Also, \hat{h}_n is the interface displacement of the bottom of layer n from its mean position.

In matrix notation, (1)–(3) can be written

$$\mathbf{L}\Phi = -\frac{1}{c^2}\Phi. \quad (5)$$

Here \mathbf{L} is a matrix containing the operators in the first two terms of (1) and (2) and the first term in (3) and Φ is a vector

containing the vertical structure of the streamfunction for a particular mode. Equation (5) is solved as an eigenvalue problem for c^{-2} . The eigenvectors are sorted by their phase speeds, with the most rapid phase speed being the barotropic mode. In run 2, for the first two baroclinic modes the structure is smooth and shows no obvious discontinuities that would suggest lack of vertical resolution (Fig. 4 ) , while the third baroclinic mode starts to show the finite number of layers in the calculation. Note that the density resolution is concentrated in the upper 500 m. The phase speed of the first baroclinic mode gravity wave shows reasonable correspondence with other calculations (cf. Killworth et al. 1997), although it is slightly larger than their estimate based on the Levitus et al. data.

Since the higher vertical modes are not well represented by the limited vertical resolution in the model, we will concentrate our discussion on the response in the barotropic and the first two baroclinic modes. We have ignored the impact of vertical shear on the modal structure and phase speeds. According to the calculation of Killworth et al. (1997), the modal structure for the first baroclinic mode is relatively uninfluenced by the zonal vertical shear, although the phase speed can differ from the traditional phase speed by as much as factor of 2. For the analysis done here, we do not use the phase speed directly, so our results should be relatively robust to the exclusion of the mean flow field, particularly for the first baroclinic mode. In addition, with the inclusion of the mean flow, the modes are no longer complete or orthogonal.

First, we decompose the SSH response using the vertical structure of the streamfunction anomalies to determine how each mode contributes to the SSH variations. Since the vertical modes are orthogonal and complete by construction, we can write the streamfunction in any layer and at any point as a sum of contributions from each vertical mode:



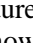
$$\Psi = \mathbf{R}\mathbf{a}, \quad (6)$$

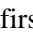
where \mathbf{R} is the matrix whose columns are made up of the eigenvectors Φ that represent the vertical structure of each mode and \mathbf{a} is a vector that represents the time-dependent magnitude of each mode. The vector Ψ contains the model streamfunction as a function of time. At each time step \mathbf{a} is found from (6) and the model streamfunction deviations using

$$\mathbf{a} = \mathbf{R}^{-1}\Psi. \quad (7)$$

To determine the contribution to the sea surface height for each mode, we find how much each vertical mode contributes to the stream function in layer 1. There the streamfunction is related to the SSH (η) by

$$\eta = \frac{g}{f_0}\psi_1 = \frac{g}{f_0} \sum_{j=1,m} R_{1j}a_j. \quad (8)$$

To study how each mode contributes to the SSH, we examine $R_{1j}a_j$ for $j = 1, 3$ (the barotropic and first two baroclinic modes). Each of the vertical modes contributes different spatial and temporal structure to the SSH response. The barotropic mode is quite noisy, but does show structure consistent with a barotropic Sverdrup-like response as a zonally uniform and nonpropagating signal (Fig. 5a ) . The first baroclinic mode shows propagation and is the mode that we identify with Rossby waves that appear so strongly in the observations (Fig. 5b ) . The second baroclinic modes have slower propagation and a weaker response (Fig. 5c ) . The contribution to the SSH from the first baroclinic mode shows western intensification and has similar structure to that found by VKT while the second baroclinic mode is larger in the Kuroshio Extension and subpolar gyre (not shown).

The modal decomposition for runs 2, 3, and 4 shows the destructive interference of the Ekman pumping and diabatic pumping response (Fig. 6 ) . The first baroclinic mode response in run 4 is larger than the response in run 2 or in run 3. This suggests that the wind-driven response and the diabatic response destructively interfere to lower the total (run 2) response. This interference is largest between 20° and 35°N. In contrast, for the second baroclinic mode there is constructive interference poleward of 25°N. Note that the second baroclinic mode response is larger than the first baroclinic mode response under thermodynamic forcing alone (run 3) since its vertical structure projects better onto the thermodynamic forcing.

To determine how the diapycnal processes influence each vertical mode in the model, a dynamical interpretation must be made. To do this, we use quasigeostrophic theory. We have assumed that the motion is linear and has large horizontal length scales so that the relative vorticity can be ignored. Mixing is written as a diapycnal flux at the top and bottom of each layer. The continuity equation for each layer can then be written as

$$\frac{\partial}{\partial t}h_n + \nabla \cdot (\mathbf{u}_n h_n) = w_{n-1} - w_n, \quad (9)$$

where h_n is the thickness of layer n and w_n is the diabatic velocity or flux across the interface at the bottom of layer n .

The linear layer quasigeostrophic potential vorticity (PV) equations are

$$\frac{\partial}{\partial t} \left(\frac{\psi_2 - \psi_1}{H_1 g_1} - \frac{\psi_1}{H_1 g} \right) + \beta \frac{\partial \psi_1}{\partial x} = \frac{f}{H_1} (w_{\text{EK}} - w_1) \quad (10)$$

for layer 1,

$$\begin{aligned} \frac{\partial}{\partial t} \left(\frac{\psi_{n+1} - \psi_n}{H_n g_n} + \frac{\psi_{n-1} - \psi_n}{H_n g_{n-1}} \right) + \beta \frac{\partial \psi_n}{\partial x} \\ = \frac{f}{H_n} (w_{n-1} - w_n) \end{aligned} \quad (11)$$

for interior layers, and

$$\frac{\partial}{\partial t} \left(\frac{\psi_{m-1} - \psi_m}{H_m g_{m-1}} \right) + \beta \frac{\partial \psi_m}{\partial x} = \frac{f}{H_m} w_{m-1} \quad (12)$$

for the bottom layer.

In setting up (10)–(12), we have assumed that the Ekman layer is much thinner than the mixed layer so that the mean mixed layer can be treated as layer one in the above equations. This means that the Ekman pumping acts on the top of the first layer. This is not strictly accurate since in the model the wind acts as a body force in the mixed layer; thus the mixed layer and Ekman layer are the same depth. Treating the mixed layer with separate dynamics from the interior layers would introduce additional complexity and is not warranted here. Note that Ekman pumping in the layered model is not a diabatic vertical velocity in that it does not cause fluid to pass between layers; thus it does not appear in the diapycnal velocity diagnosed from the model. It does, however, directly modify PV in the top layer. In contrast, the diapycnal velocity causes mass redistribution between the layers, and affects the PV in each layer. In this case, most of the diapycnal mixing comes about from entrainment and detrainment at the base of the mixed layer. The interior diapycnal velocities that are diagnosed from the model are assigned to the appropriate interface when layers vanish using the same algorithm as described above for the construction of the interface deviations. We also continue to ignore vertical shear in the background flow field.

The PV equations for each layer (10)–(12) can be written

$$\mathbf{L} \frac{\partial \Psi}{\partial t} + \beta \frac{\partial \Psi}{\partial x} = \mathbf{F}, \quad (13)$$

where Ψ is a vector representing the streamfunction in each layer and \mathbf{F} is the rhs of (10)–(12).

To transform (13) to PV equations for each vertical mode, we first note that we can write (5) as

$$\mathbf{L}\mathbf{R} = -\mathbf{R}\mathbf{C}, \quad (14)$$

where \mathbf{C} is a matrix containing the eigenvalues (c^{-2}) of (5) as elements of the diagonal. Then we can write (14) as

$$\mathbf{H}\mathbf{L}\mathbf{R} = -\mathbf{H}\mathbf{R}\mathbf{C}, \quad (14)$$

where \mathbf{H} is a matrix whose diagonal elements are the thickness of each layer. If we then take the transpose of each side of (14), we find that

$$\mathbf{R}^T \mathbf{H} \mathbf{L} = -\mathbf{C} \mathbf{R}^T \mathbf{H} \quad (15)$$

since $\mathbf{H}\mathbf{L}$ is symmetric (this is another way of saying that the operator is self-adjoint). Thus, we can transform (13) by multiplying by $\mathbf{R}^T \mathbf{H}$ and using (15) to get

We have created an equation that defines the propagation and forcing of the potential vorticity for each vertical mode, in terms of the vertical divergences (\mathbf{F}) where now the j th element of $\mathbf{R}^T \mathbf{H} \Psi$ is the potential vorticity of the j th vertical mode. We have assumed that \mathbf{R} and \mathbf{H} are independent of time and that they vary slowly in the zonal direction.

The rms contribution of the Ekman pumping and diapycnal velocities to the PV forcing of each vertical mode as calculated from the rhs of (16) can then be compared (Fig. 7). For the first baroclinic mode, the Ekman pumping dominates everywhere, while diapycnal pumping plays an important role between 30° and 40°N near the Kuroshio Extension (Fig. 7a). The diabatic pumping is large just in the region where there is the largest difference between the wind only run and the control run (cf. Fig. 7 to Fig. 3). For the second baroclinic mode, Ekman pumping and diabatic pumping are coincident and of similar magnitude with the maximum in the Kuroshio Extension (Fig. 7b). One would not expect a one-to-one correspondence between the energy in the modes and the forcing patterns. Rossby wave energy locally depends on the accumulation of forcing as the Rossby wave propagates to the west.

We can define a transfer coefficient for Ekman pumping for each vertical mode taken from (16) that determines the magnitude of the forcing for mode given by $f_0 \Phi_n(0) c_n^2$. A question arises whether the changes in the stratification in the various experiments that were discussed in section 3 could explain the changes in the amplitude of the response rather than diapycnal pumping. The ratio of the transfer coefficient for run 2 and run 4 shows that the expected wind-driven response is approximately the same in both runs (Fig. 8). However, the ratio of the response is significantly different at midlatitudes, confirming the role of diapycnal pumping in the evolution of the first baroclinic mode.

There is no guarantee that diapycnal forcing will cause damping (see, e.g., Liu 1999). To ascertain its effect on the first baroclinic mode more directly, we solve the one-dimensional wave equation (16) using the forcing fields calculated from its right-hand side and the phase speed calculated from the modal analysis. The equation is solved by an upwind differencing scheme and then is compared against the modal calculation. In general, the amplitude found from the one-dimensional model is about a factor of 2 smaller than found from the modal analysis. This can be explained by the errors in the wave equation associated with the presence of the mean flow related to the factor-of-2 difference in the phase speed from that of a resting ocean at midlatitudes (as show by Killworth et al. 1997). Barring the differences in amplitude, south of 30°N, the wave equation reproduces the modal time/longitude behavior and it is well correlated with the results from the numerical model (Fig. 8). Between 17° and 28°N, the diapycnal pumping response is anticorrelated with the Ekman pumping response, resulting in a total wave field that is smaller than the wave field forced by Ekman pumping alone.

There are several caveats that should be made about this analysis. In the modal analysis, we have linearized about the mean stratification, which does not take into account the order one changes in the density structure that occur throughout the year in the upper ocean. The one-dimensional model does not do very well in predicting the response of the full model poleward of 45° where the annual Rossby wave is most likely evanescent, and VKT found very little Rossby wave response. In this region we expect that the one-dimensional model should fail. In addition, in this region the mean flow is strongly eastward, and the wave propagation characteristic would be significantly modified so that the one-dimensional model would not be valid.

The higher vertical modes are strongly influenced by diapycnal processes in this analysis, which suggests that they would be strongly forced by diapycnal processes, much more so than by Ekman pumping. However, the higher modes are less well represented in the model, and the mean velocity field is more important in their evolution than it is for the first baroclinic mode. The effects of the mean flow on the propagation characteristics of the higher modes will be explored in a subsequent paper.

5. Conclusions

Model simulations of the SSH response to wind forcing show that diapycnal processes and mixed layer evolution are important in the dynamics of the SSH response, particularly at mid- to high latitudes. Typically the propagation of the first baroclinic mode Rossby waves has been studied in simple models without the inclusion of diapycnal processes and mixed layer physics, and thus the adjustment of the ocean to seasonal changes in wind stress has been decoupled from the seasonal cycle of heating and cooling. The simulations show that, in particular, the presence of the seasonal cycle mixed layer entrainment/detrainment can be important in oceanic adjustment at midlatitudes. In an adiabatic simulation (run 1), Rossby waves forced near the eastern boundary propagate without reduction in amplitude, and an obvious seasonal cycle is lost. In contrast, in run 2 Rossby waves are less vigorous. We argue here that the mixed layer seasonal cycle, and the associated diapycnal velocities, is important for changing the Rossby waves.

A modal decomposition of the model interface displacements shows that, as expected, the barotropic mode dominates the SSH signal at high latitudes, with the first baroclinic mode important at mid to low latitudes and higher vertical modes not

contributing as much. The model decomposition shows that the first baroclinic mode is suppressed at midlatitudes by diapycnal pumping. In contrast, the second baroclinic mode is enhanced by diapycnal pumping.

The results from a one-dimensional wave equation are consistent with the modal analysis and show that the diabatic response and Ekman pumping response are opposite between 17° and 28°N for the first baroclinic mode. The resulting signal is weaker than the Ekman pumping signal alone. In addition, the one-dimensional model has good predictive skill south of 30°N, while north of 45°N, the skill is very poor indeed, suggesting that the linearized potential vorticity equation is not valid in this region. A more complete analysis would include the effects of the mean flow on the propagation pathways of the waves.

Higher resolution in the model, both vertical and horizontal, would help with a more faithful representation of the observations. In particular, the choice of density resolution influences how well the stratification can be represented. The vertical structure in these model simulations was chosen to maximize resolution in the subtropics, which leaves the resolution in the Tropics lacking near the surface. This leads to mixed layers that are too deep, and vertical mixing that is unrealistically large. Likewise, the lack of horizontal resolution affects the northwestern Pacific, where the Kuroshio Extension is too far north, and where the mixed layers are too deep.

This study shows that Rossby waves, which are traditionally thought to be purely adiabatic, can be greatly influenced by diabatic processes. This has been explored for decadal variability (Liu 1999), but it is on the seasonal cycle that the dynamic impact of diapycnal velocity associated with the seasonal cycle of heating and cooling is the largest.

Acknowledgments

We acknowledge the TOPEX/Poseidon Extended Mission project at JPL and D. Chelton and M. Schlax for mapped altimetric fields. We thank Helma Lindow for some early model runs. Funding was provided by NASA Contract 960888 with the Jet Propulsion Laboratory (TOPEX/Poseidon Extended Mission Science Working Team) and an NSF grant to Thompson and Kelly.

REFERENCES

- Bleck R., H. P. Hansen, D. Hu, and E. B. Kraus, 1989: Mixed layer–thermocline interaction in a three-dimensional isopycnic coordinate model. *J. Phys. Oceanogr.*, **19**, 1417–1439. [Find this article online](#)
- Chelton D. B., and M. G. Schlax, 1996: Global observations of oceanic Rossby waves. *Science*, **272**, 234–238. [Find this article online](#)
- da Silva A. M., C. C. Young, and S. Levitus, 1994: *Algorithms and Procedures*. Vol. 1, *Atlas of Surface Marine Data 1994*, NOAA Atlas NESDIS 6, 51 pp.
- Greatbatch R. J., 1994: A note on the representation of steric sea level in models that conserve volume rather than mass. *J. Geophys. Res.*, **99**, 12767–12771. [Find this article online](#)
- Hallberg R., 2000: Time integration of diapycnal diffusion and Richardson number dependent mixing in isopycnic coordinate ocean models. *Mon. Wea. Rev.*, **128**, 1402–1419. [Find this article online](#)
- Hallberg R., and P. Rhines, 1996: Buoyancy-driven circulation in an ocean basin with isopycnals intersecting the sloping boundary. *J. Phys. Oceanogr.*, **26**, 913–940. [Find this article online](#)
- Killworth P. D., and J. R. Blundell, 1999: The effect of bottom topography on the speed of long extratropical planetary waves. *J. Phys. Oceanogr.*, **29**, 2689–2710. [Find this article online](#)
- Killworth P. D., D. B. Chelton, and R. A. deSzoeke, 1997: The speed of observed and theoretical long extratropical planetary waves. *J. Phys. Oceanogr.*, **27**, 1946–1966. [Find this article online](#)
- Kraus E. B., and J. S. Turner, 1969: A one-dimensional model of the seasonal thermocline: II. The general theory and its consequences. *Tellus*, **19**, 98–105. [Find this article online](#)
- Ladd C., and L. Thompson, 2001: Water mass formation in an isopycnic model of the North Pacific. *J. Phys. Oceanogr.*, **31**, 1517–1537. [Find this article online](#)
- Levitus S., and T. P. Boyer, 1994: *Temperature*. Vol. 4, *World Ocean Atlas 1994*, NOAA Atlas NESDIS4, 117 pp.
- Levitus S., R. Burgett, and T. Boyer, 1994: *Salinity*. Vol. 3, *World Ocean Atlas 1994*, NOAA Atlas NESDIS 3, 99 pp.

Liu Z., 1999: Forced planetary wave response in a thermocline gyre. *J. Phys. Oceanogr.*, **29**, 1036–1055. [Find this article online](#)

Marshall J., and F. Schott, 1999: Open-ocean convection: Observations, theory and models. *Rev. Geophys.*, **37**, 1–64. [Find this article online](#)

Murdegudde R., M. Cane, and V. Prasad, 1995: A reduced-gravity, primitive equation, isopycnal ocean GCM: Formulation and simulations. *Mon. Wea. Rev.*, **123**, 2864–2887. [Find this article online](#)

New A. L., R. Bleck, Y. Jia, R. Marsh, M. Huddleston, and S. Barnard, 1995: An isopycnal model study of the North Atlantic. Part I: Mode experiment. *J. Phys. Oceanogr.*, **25**, 2667–2669. [Find this article online](#)

Qiu B., W. Miao, and P. Muller, 1997: Propagation and decay of forced and free baroclinic Rossby waves in off-equatorial oceans. *J. Phys. Oceanogr.*, **27**, 2405–2417. [Find this article online](#)

Rothstein L. M., R. H. Zhang, A. J. Busalacchi, and D. Chen, 1998: A numerical simulation of water pathways in the subtropical and tropical Pacific Ocean. *J. Phys. Oceanogr.*, **28**, 322–343. [Find this article online](#)

Stammer D., 1997: Steric and wind-induced changes in TOPEX/POSEIDON large-scale sea surface topography observations. *J. Geophys. Res.*, **102**, 20987–21009. [Find this article online](#)

Stammer D., R. Tokmakian, A. Semtner, and C. Wunsch, 1996: How well does a 1/4 degree global circulation model simulate large-scale oceanic observations? *J. Geophys. Res.*, **101**, 25779–25811. [Find this article online](#)

Vivier F., Kelly K. A., and L. Thompson, 1999: The contributions of waves, wind forcing, and surface heating to sea surface height observations of the Pacific Ocean. *J. Geophys. Res.*, **104**, 20767–20784. [Find this article online](#)

APPENDIX

6. The Mixed Layer Formulation

The model uses a bulk [Kraus–Turner \(1969\)](#) type mixed layer, much like that of [Bleck et al. \(1989\)](#) except that a variable density buffer layer is used to receive the fluid detrained from the mixed layer.

The mixed layer depth is determined by energy considerations. If there is turbulent kinetic energy available to drive mixed layer deepening, it does so entraining successively from the lightest layers that contain any mass. Alternately, if there is net surface loss of buoyancy, the mixed layer may entrain due to free convection. Otherwise, the mixed layer detrains to the Monin–Obukhov depth—the depth at which wind generated turbulent kinetic energy balances the work required to mix the surface buoyancy forcing throughout the mixed layer.

Fluid that is detrained from the mixed layer goes into a variable density buffer layer. This avoids the necessity of having a “fossil mixed layer” that is appended to the real mixed layer, as in [Bleck et al. \(1989\)](#). The details of this buffer layer differ from those of [Murdegudde et al. \(1995\)](#), but the layer is conceptually similar. For example, the scheme described here conserves heat while Murdegudde's does not. If there is an isopycnal layer that is intermediate in density between the mixed layer and the buffer layer, it is possible to split the buffer layer while maintaining a stable density profile. Bleck et al. are careful to insure that the fossil mixed layer does not alter the surface temperature or salinity tendency due to vertical processes. But mixed layer thickness, temperature, and salinity tendencies due to horizontal advection within the mixed layer are unavoidably affected by the presence of a fossil mixed layer. The mixed layer/buffer layer approach used here gives a more accurate representation of the effects of horizontal advection on the mixed layer properties.

The specific calculation of the one-dimensional mixed layer evolution is as follows.

1. If there is a net surface loss of buoyancy from the ocean, the mixed layer becomes denser.
2. The water column convectively adjusts. Any mass in layers lighter than the mixed layer is entrained into the mixed layer. Penetrative convection seems to be fairly unimportant in the ocean ([Marshall and Schott 1999](#)), so none of the potential energy released through convective adjustment is retained to drive further entrainment.
3. As prescribed by [Kraus and Turner \(1969\)](#) or [Bleck et al. \(1989\)](#), turbulent kinetic energy (with a specified surface source) is used to drive mixed layer entrainment if there is a net surface buoyancy loss or if the mixed layer is shallower than the Monin–Obukhov depth, $h_{MO} = 2m_0 u_*^3 / B_0$. Here u_* is the surface friction velocity, B_0 is the total

surface buoyancy flux into the ocean and m_0 is a nondimensional constant, 0.5. The entrainment is essentially the same as described in Bleck et al. The mixed layer entrains from successively denser layers until the increase in the potential energy due to the entrainment equals the surface energy available to drive mixing:

$$\text{TKE} = \Delta t \left\{ m_0 u_*^3 - \frac{h_0}{4} [(B_0 + |B_0|) + n(B_0 - |B_0|)] \right\}, \quad (\text{A1})$$

where Δt is the time increment, h_0 is the mixed layer thickness at the start of the entrainment, and n is another nondimensional constant, here 0.03. It is easy to show that the potential energy increase due to an increment Δh of entrainment by the mixed layer is

$$\Delta \text{PE} = \frac{1}{2} h_0 \Delta h (b_{\text{ML}} - b_{\text{Ent}}), \quad (\text{A2})$$

where b_{ML} is the mixed layer buoyancy and b_{Ent} is the buoyancy of the entrained fluid. Entrainment continues until $\Delta \text{PE} = \text{TKE}$. The surface TKE available to drive mixing does not decay with depth in the current model.

4. If the mixed layer is deeper than the Monin–Obukhov depth, the mixed layer detrains into the buffer layer until the mixed layer thickness agrees with the Monin–Obukhov depth and the mixed layer buoyancy increases due to any net positive buoyancy forcing.
5. If there is an isopycnal layer that is intermediate in density between the buffer layer and the mixed layer (and there is any fluid in the buffer layer), the buffer layer is detrained. It is partitioned into a portion that matches the density of the intermediate density layer and a portion that matches the density of the next denser layer. If layer k is intermediate in density between the buffer layer and the mixed layer, the amount of fluid that goes into layers k and $k + 1$ is, respectively,

$$\omega_{k+1} = h_B \frac{\rho_B - \rho_k}{\rho_{k+1} - \rho_k} \quad \text{and}$$

$$\omega_k = h_B \frac{\rho_{k+1} - \rho_B}{\rho_{k+1} - \rho_k}. \quad (\text{A3})$$

Whenever fluid moves across interfaces between layers (except during the partitioning of the buffer layer), it does so with the velocity and tracer concentrations of the layer from where it came.

The mixed layer and buffer layer obey the same momentum equations as all of the interior isopycnal layers, except for the inclusion of an additional pressure gradient term. When the momentum equations,

$$\begin{aligned} \frac{\partial \mathbf{u}}{\partial t} + (f\hat{k} + \nabla_s \times \mathbf{u}) \times \mathbf{u} \\ = -\nabla_s \left(\frac{p}{\rho} + gz + \frac{1}{2} \mathbf{u} \cdot \mathbf{u} \right) \\ - \frac{p}{\rho^2} \nabla_s \rho + \text{viscosity} \end{aligned} \quad (\text{A5})$$

(written in standard notation, with the subscript S emphasizing that the gradients are taken along coordinate surfaces, and only the horizontal components of the velocities are used, consistent with the hydrostatic

approximation), are evaluated in layers of nonconstant density, the middle term on the right-hand side does not vanish.

The average through the layer of this term is

$$-\overline{\frac{p}{\rho^2} \nabla_s \rho} \approx -\frac{g}{\rho_0} \left(\eta + \frac{h}{2} \right) \nabla_s \rho, \quad (\text{A6})$$

where η is the height of the interface above the layer and h is the thickness of the layer. The natural expression of this term on a C grid is not obvious, but a finite-element interpretation suggests the discretization

$$-\frac{g}{\rho_0} \left(\eta + \frac{h}{2} \right) \frac{\partial \rho}{\partial x} \Big|_s \approx -\frac{g}{\rho_0} \frac{h^+ h^- + \eta^+ h^- + \eta^- h^+}{h^+ + h^-} \frac{\rho^+ - \rho^-}{\Delta x}, \quad (\text{A7})$$

where the superscripts + and - indicate the points to the east and west of the velocity point where this term is being evaluated. This discretization is used in the mixed layer calculations.

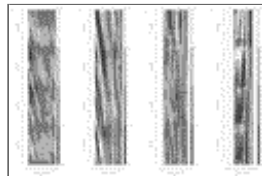
Tables

Table 1. Simulations

Layer	Density
Adiabatic	
1	1021.5
2	1023.5
3	1024.5
4	1026.0
5	1026.75
6	1027.25
7	1027.25
Diabatic	
1 (mixed layer)	1022.8
2 (buffer layer)	1022.9
3	1023.5
4	1024.5
5	1025
6	1025.5
7	1026
8	1026.5
9	1027.5
10	1028

[Click on thumbnail for full-sized image.](#)

Figures



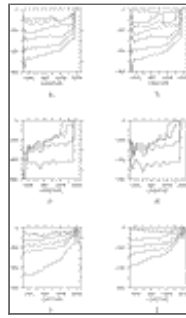
[Click on thumbnail for full-sized image.](#)

FIG. 1. Time-longitude plots model of SSH for years 1993–96 at 10°, 20°, 30°, and 40°N: (a)–(d) adiabatic simulation (run 1) (contour interval 10 cm), and (e)–(h) diabatic simulation (run 2) (contour interval 5 cm).



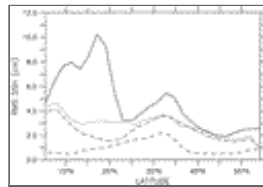
Click on thumbnail for full-sized image.

FIG. 1. (Continued)



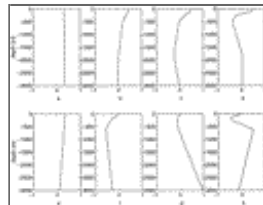
Click on thumbnail for full-sized image.

FIG. 2. Layer interfaces at 22°N for winter and summer: (a) and (b) run 2, (c) and (d) run 1, and (e) and (f) [Levitus et al. \(1994\)](#) observations. Mixed layer base is shown in (a) and (b) and (e) and (f) as a dark line



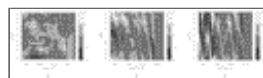
Click on thumbnail for full-sized image.

FIG. 3. Rms SSH anomaly (cm) zonally averaged. Solid line is run 1, dot-dashed is run 2, dashed line is run 3, and small dotted line is run 4



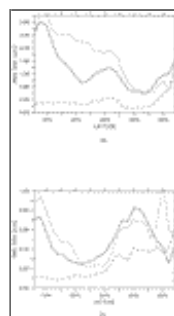
Click on thumbnail for full-sized image.

FIG. 4. Nondimensional vertical structure for the first four vertical modes from run 2 in (a)–(d) streamfunction and (e)–(h) interface displacement at 22°N, 180°



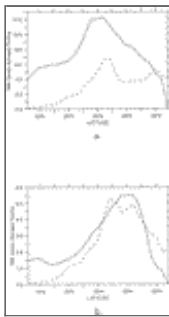
Click on thumbnail for full-sized image.

FIG. 5. Time–longitude plots for contributions at 22°N to SSH anomaly for year 1992 from run 2 for each of the vertical modes: (a) barotropic mode (contour interval 1.25 cm), (b) first baroclinic mode (contour interval 1.25 cm), and (c) second baroclinic mode (contour interval 0.375 cm).



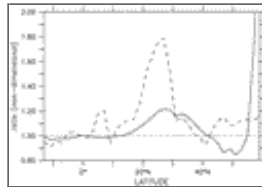
Click on thumbnail for full-sized image.

FIG. 6. Zonally averaged rms SSH anomaly (cm) from each vertical mode from run 2 (solid), run 3 (dashed), and run 4 (dotted): (a) first baroclinic mode and (b) second baroclinic mode



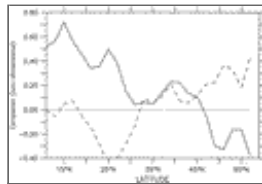
[Click on thumbnail for full-sized image.](#)

FIG. 7. Rms contribution to the forcing of the baroclinic modes by Ekman pumping (solid) and diabatic pumping (dashed) in run 2: (a) first baroclinic mode and (b) second baroclinic mode



[Click on thumbnail for full-sized image.](#)

FIG. 8. Ratio of transfer coefficient. Solid line is ratio of transfer coefficient of the run 4 to run 2 (zonally averaged), and dashed line is the ratio of rms SSH of run 4 to run 2 (zonally averaged)



[Click on thumbnail for full-sized image.](#)

FIG. 9. Correlation coefficients between first baroclinic mode response in the numerical model run 2 and that from the 1D wave equation (solid line), and correlation coefficient between the the diabatic pumping response and the Ekman pumping response from the 1D wave equation (dashed line)

Corresponding author address: Dr. LuAnne Thompson, School of Oceanography, University of Washington, Box 355351, Seattle, WA 98195-5351. E-mail: luanne@ocean.washington.edu

[top ▲](#)



© 2008 American Meteorological Society [Privacy Policy and Disclaimer](#)
 Headquarters: 45 Beacon Street Boston, MA 02108-3693
 DC Office: 1120 G Street, NW, Suite 800 Washington DC, 20005-3826
amsinfo@ametsoc.org Phone: 617-227-2425 Fax: 617-742-8718
 Allen Press, Inc. assists in the online publication of AMS journals.